Paving the Way for A Sustainable and Efficient SiO₂/TiO₂ Photocatalytic Composite

Mattia Pierpaoli [1,*] , Xu Zheng [2], Vladimir Bondarenko [1], Gabriele Fava [1] and Maria Letizia Ruello [1]

[1] Department of Materials, Environmental Sciences and Urban Planning, Università Politecnica delle Marche, Via Brecce Bianche 12, 60131 Ancona, Italy

[2] School of Civil Engineering and Architecture, Zhejiang Sci-Tech University, Hangzhou 310018, China

*   Correspondence: m.pierpaoli@pm.univpm.it

Abstract: Although photocatalysis is an extraordinary and tremendously explored topic, there is a need to find new ways to encourage the production of composite materials that are economical, efficient and with limited environmental impact. Nanocatalysts may benefit from appropriate support material for many reasons. In this study, TiO₂ was deposited on SiO₂, so that the silica not only provides the macroscopic structure on which the TiO₂ is formed, but it positively affects the photocatalytic activity as well. This is because of the greater specific surface area which favors the adsorption of pollutants near the photocatalyst, the higher amount of surface-adsorbed water and hydroxyl groups and the inhibition of the photogenerated electron-hole recombination. The choice of preparing the Ti-precursor starting from titanium shavings and to directly deposit TiO₂ on micrometric-sized silica by a simple hydrothermal method highlights the process sustainability. The results showed that it is possible to produce a photocatalytic composite from secondary materials, exhibiting excellent photocatalytic properties, comparable to the pristine one, and opening the possibility for large-scale production.

Keywords: SiO₂/TiO₂ composite; photocatalysis; NOx; MEK; adsorption; de-polluting

1. Introduction

The main strength of environmental photocatalysis is that it can mineralize dangerous pollutants in harmless compounds, ideally without the expenditure of energy. However, researchers have to keep in mind how to optimize the process in order to obtain the most effective, efficient, stable, inexpensive and sustainable photocatalyst. Since it is not always possible to achieve all these characteristics simultaneously, it is necessary, instead, to look for compromises that do not excessively undermine one, or more, of these.

Among different photocatalysts, titanium dioxide (TiO₂) is one of the most investigated materials in the last decades, because of its chemical and mechanical stability, high-efficiency, nontoxic nature, and it is relatively inexpensive. However, the production costs for titanium dioxide are relatively high [1]. The sulfate and the chloride routes are two industrial processes to produce TiO₂ pigments from the ilmenite mineral, and they are demanding in terms of chemical reagents, energy, and waste products [1,2]. The synthesis of nanostructured titanium dioxide for photocatalytic applications can be pursued by different methods: Sol-gel; chemical and physical vapor deposition; hydrothermal and solvothermal; spray pyrolysis; sonochemical and microwave-assisted vapor deposition; electrophoretic deposition; Ti-metal oxidation; and electrochemical anodization. It is noted that a few of the listed above processes allow obtaining a nanostructured TiO₂ directly over a titanium metallic support. However, with consequent economic and process improvements, the deposition of TiO₂ over a different support

material, in order to improve the adsorbing properties of the composite, is generally restricted by using different titania precursors. As the nano-titania particles have a diameter of tens of nanometers, it is necessary to have an appropriate matrix to support them. Moreover, the formation of chemical bonds between the titania and the substrate may result in a enhanced photocatalytic activity and a broader spectral response [3–6]. Furthermore, the higher specific surface area of the support material results in a more efficient photocatalytic process, as the pollutant is adsorbed into the vicinity of the photocatalyst. For these reasons, the support material plays a fundamental role in the overall process in terms of costs, efficiency, reliability, and sustainability.

Silicon dioxide (SiO_2) is a widely diffused, low-cost, resistant to high temperatures, adsorbent, non-toxic material. The publication in 1968 by Stöber et al. on the controlled growth of monodisperse silica spheres in the micron size range [7] fueled the research of silica-coated catalysts, leading to an exponential growth of the scientific literature on the subject (Figure S1, in the supplementary file). Since the production cost of silica is lower than that of titania, the realization of composite material makes it possible to obtain a cheaper photocatalytic material, which benefits from the de-polluting and self-cleaning properties of titania, and the adsorptive and mechanical properties of silica.

Table 1 reports some of the most relevant research focused on the removal of specific pollutants, with different SiO_2/TiO_2 synthesis methods.

Table 1. A comparison of the synthesis type and relative precursor for relevant studies about SiO_2/TiO_2 composites.

Author	Year	Synthesis Type	TiO_2 Precursor	SiO_2 Precursor	Objective	Ref.
Anderson et al.	1997	sol-gel	TTIP	TEOS	Decomposition of salicylic acid	[8]
Dutoit et al.	1995	sol-gel	TTIP	TMOS	Epoxidation of olefins.	[9]
Fu et al.	1996	sol−gel	TTIP	TEOS	Oxidation of ethylene	[10]
Aguado et al.	2006	sol-gel	TTIP	TEOS	Oxidation of potassium cyanide	[11]
Kochkar et al.	1997	sol-gel	TTIP	TEOS	Epoxidation of cyclohexene	[12]
Li et al.	2013	sol-gel	TTIP	TEOS	Degradation of MB	[13]
Guo et al.	2014	sol-gel	TBOT	TEOS	Degradation of azo dyes and phenol	[14]
Dong et al.	2007	sol-gel	TTIP	TEOS	Degradation of RhB	[15]
Li et al.	2005	sol-gel	$TiCl_4$	Na_2SiO_3	Degradation of benzene	[16]
Beyers et al.	2009	sol-gel	TTIP	TEOS	Degradation of Rh6G	[17]
Van Grieken	2002	sol-gel	TTIP	SiO_2,TEOS	Cyanide oxidation	[18]
Itoh et al.	1974	sol-gel	$TiCl_4$	TEOS	amination of phenol and hydration of ethylene.	[19]
Nilchi et al.	2010	sol-gel	$TiCl_4$	TEOS	degradation of Congo Red (CR) azo dye	[20]
Yang et al.	2016	sol-gel, hydro-calcination, co-precipitation, solid-phase synthesis	TBOT	TEOS	Degradation of MB, RhB, methyl violet, naphthol green B, basic fuchsin, malachite green, and methyl red	[21]

Table 1. *Cont.*

Author	Year	Synthesis Type	TiO$_2$ Precursor	SiO$_2$ Precursor	Objective	Ref.
Zhang et al.	2005	sol-gel	TTIP	TEOS	Degradation of methyl orange	[22]
Xie et al.	2004	sol-gel	TBOT	TEOS	Oxidation of heptane	[23]
Bellardita et al.	2010	Impregnation	TiCl$_4$	SiO$_2$,flyash	NOx abatement and for 4-nitrophenol photodegradation	[24]
Belhekar et al.	2002	Impregnation	TBOT	TEOS	Degradation of MB,	[25]
Leboda et al.	1999	CVD	TiCl$_4$	SiO$_2$		[26]
Zhijie et al.	2005	hydrothermal	TBOT	TEOS	Decomposition of MB	[27]
Anpo et al.	1986	coprecipitation	TiCl$_4$	TEOS		[28]
He et al.	2010	templating method	TBOT	TEOS	Degradation of Rh6G	[29]
Inumaru et al.	2005	precipitation	P25	TEOS	Decomposition of alkylphenols	[30]
Paušová et al.	2014	Wet mixing	TiCl$_4$	SiO$_2$	decomposition of Acid, MB, hexane	[31]
Smitha et al.	2010	sol-gel	TiOSO$_4$	TEOS	Degradation of MB	[32]
Alaoui et al.	2009	SiO$_2$-entrapment method	P25	Sodium silicate	Degradation of indigo carmine	[33]
Hirano et al.	2004	hydrothermal	TiOSO$_4$	TEOS	Degradation of MB, NO	[34]
Montes et al.	1997	Precipitation, hydrolysis	TiCl$_3$	TEOS	Catalyst of n-butane-hydrogen reactions	[35]

Titanium isopropoxide (TTIP), tetrabutyl titanate (TBOT), tetraethoxysilane (TEOS), tetramethyl orthosilicate (TMOS), rhodamine B (RhB), rhodamine 6G (Rh6G), methylene blue (MB), nitrogen oxide (NO).

As it is possible to observe, the sol-gel method is the most adopted method. Among the different preparation methods, sol-gel hydrolysis allows to control the textural and surface properties of the mixed oxides. However, the use of silica precursors, which allows to have a controlled growth of silica particles, moves away from the principle of minimizing production costs, and it is not an easily scalable method for larger productions, such as the building industry. Similarly, the use of titanium precursors, such as titanium isopropoxide (TTIP) [8–13,15,17,18,22] tetrabutyl orthotitanate (TBOT) [14,21,25,27], titanyl sulphate (TiOSO$_4$) [32,36,37], titanium tetrachloride (TiCl$_4$) [16,20,24,26,31], titanium(III) trichloride (TiCl$_3$) [35] are unsuitable as well, due to their cost or difficulty in the preparation method. While tetraethoxysilane (TEOS) is the preferred precursor to obtain a controlled distribution of silica particles, a few authors have investigated different methods to achieve a cost-effective composite, such as using sodium silicate [16,33], a commercially-available silica [18,24,26,31] or fly ashes [24]. As the process for producing nano-sized TiO$_2$ is energy-intensive, a few authors studied the life cycle of the TiO$_2$-nanoparticles manufacturing process [38–40], with a particular focus on the energy streams. As sustainability is the main concern, the use of secondary raw material, or waste material, is to be preferred instead of a pristine one.

In this study, nanosized anatase TiO$_2$ has been deposited on macroscopic silica. The uniqueness of this study is that a SiO$_2$/TiO$_2$ composite was produced using an alternative sulfate method, starting from metallic titanium shavings and silica gel, and the composite was tested for the degradation of characteristic gaseous compounds. The choice of using a waste material (the titanium shavings) and a low-cost one (the silica) can be explained by the need to produce a composite to be used for photocatalytic mortars and plasters [41]. For this reason, commercially available silica is an effective

support material on which the deposition of a few TiO$_2$ layers is maximized, resulting in a lowered amount of titania required. Moreover, rapid reactions may be achieved by using porous catalyst support, offering a high density of active surface sites and fast molecular transport.

2. Materials and Methods

2.1. Composites Preparation

In a typical experiment, the required amount of titanium shavings (99.9% purity) was dissolved in concentrated sulfuric acid solution in a 1:10 (*w/w*) ratio, in an ultrasonic bath. The formed titanium (III) sulfate precursor, was firstly filtered with an acid-resistant filter paper and then mixed with a proper amount of water-saturated silica (in order to obtain three different TiO$_2$/SiO$_2$ ratios). The solution directly precipitated by hydrolysis was dried for a few hours in a sand bath and calcinated at 600°C in a muffle for 1 hour. Three different titania/silica ratio were obtained: 3%, 7%, 12% (*w/w*), and the composite samples were named, respectively: A3, A7, and A12. The same procedure was previously used by the authors to deposit TiO$_2$ on natural clays [42]

To compare the characteristics and the photocatalytic activity of the samples obtained by hydrothermal method, a commercially available photocatalyst, Evonik Aeroxide (formerly Degussa) P25®was added to the silica in aqueous solution, at low pH, in order to enhance the electrical attraction [40]. TiO$_2$ amounts were varied in order to obtain the same ratios for the samples obtained by the hydrothermal method, and they were named W3, W7, W12.

2.2. Composite Characterization

The pictures of every sample have been obtained by using a Keyence Digital Microscope, VHX-5000 series, jointly with a VH-Z100T Wide-range Zoom Lens (100-1000X). A SEM was performed with a Sirion200 Field-emission Scanning Electron Microscopy. An X-ray diffractometric analysis was performed using a Philips PW 1730 X-ray diffractometer. The XRD spectrum was taken from 5.0 to 50.0 2θ.

The texture properties such as surface area, pore volume, pore size distribution were tested and analyzed by an Accelerated Surface Area and Porosimetry System (ASAP2020). The system utilizes the static volumetric technique to obtain nitrogen adsorption/desorption isotherms at liquid nitrogen temperature. The surface area is calculated based on the Brunauer-Emmett-Teller (BET) equation, and pore size distributions are obtained according to the Barrett-Joyner-Halenda (BJH) theory. The experimental error of the ASAP apparatus is mainly caused by temperature and pressure transducers. The accuracy of temperature transducer is ±0.02 °C, while pressure is approximately 0.1%.

The adsorption kinetics and isotherms of testing samples on water vapor were carried out in a constant temperature and humidity chamber. The chamber can supply constant air condition with deviations of ±0.5 °C for temperature and ±3% for relative humidity. Before each test, the samples were dried at 150 °C in an oven for 4 hours. Thermal stability was earlier assessed by thermogravimetric analysis (TGA, Supplementary Material, Figure S2). The weights of the samples were recorded at set intervals by an electronic balance with an accuracy of 0.001g. To fit the experimental data, pseudo-second-order kinetics was adopted [43,44].

$$\frac{t}{q_t} = \frac{1}{h} + \frac{1}{q_e}t$$

(1)

where q_e is the amount of adsorbate (mg/g) at equilibrium, q_t is the amount of adsorbate (mg/g) at any time t, and h is the initial adsorption rate (mg/g min) as q_t/t approaches 0. In Equation (1), the pseudo-second-order model constants can be determined experimentally by plotting $\frac{t}{q_t}$ against t.

2.3. Photocatalytic Activity

The composites photocatalytic activity were assessed both by a standardized test (UNI 11247) for the nitrogen oxides (NOx) removal and by a batch test, in which methyl ethyl ketone (MEK) was used as a target volatile organic compound (VOC), representative of the indoor environments.

The experimental apparatus is illustrated in Figure 1. The reactor has a volume of 3L, and it consists of a Pyrex glass cylinder. A thin aluminum plate is positioned inside on which the powder sample is positioned. The UV lamp is located at the center of the reactor, over the sample, outside the reactor. The lamp is a UVA metal-halogen quartz lamp with mercury vapor, peak at 360 nm and adsorbed power of 400 W. The irradiance, which was measured with a photoradiometer (Delta Ohm HD 2102.2), is kept constant at 20 W/m^2. The probe of the photoradiometer is centered in the field of UVA with a resolution of 0.001 W/m^2. The NOx flux inside the reactor is kept constant with a dilution system (Calibrator 8188) which is alimented with a NOx tank (499 ppb NO). The dilution is obtained by mixing with atmospheric air at room temperature (20 °C ± 2 °C) and relative humidity between 40–50%. NOx concentrations are determined using a chemiluminescent analyzer (Monitor Labs, Nitrogen oxides analyzer model 8841).
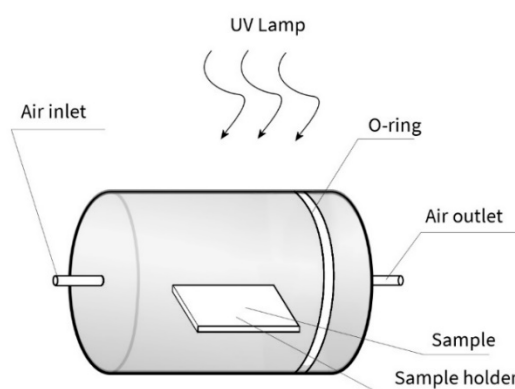

Figure 1. A schematic representation of the reactor used to determine the photocatalytic activity in NOx removal.

The concentrations were monitored in dark and light conditions. NO and NO$_x$ reduction efficiencies were evaluated as follows:

$$\text{NO removal} = \alpha \frac{NO^{dark} - NO^{light}}{NO^{dark}} \tag{2}$$

$$\text{NO}_x \text{ removal} = \alpha \frac{NO_x^{dark} - NO_x^{light}}{NO^{dark}} \tag{3}$$

where NO^{dark}, NO_x^{dark} are the initial concentrations of NO and NOx in dark condition, NO^{light}, NO_x^{light} are the concentration of NO and NO$_x$ while the UV light is turned on, and α is a correcting factor (between 0 and 1) accounting the powder exposed surface.

Methyl-ethyl-ketone (MEK) oxidation experiments have been carried out in a batch reactor. The scheme of the reactor is reported in Figure 2.

The photocatalytic reactor consists of a glass chamber having a total volume of about 1.05 L. Inside the reactor, a UV LED is present with a peak at 365 nm and adsorbed power of 1 W. The distance between the LED and the sample was taken according to the value of irradiance fixed at 7 W/m^2. Magnetic stirring guarantees air recirculation continuously. The temperature was kept constant by immersing the reactor in a thermostatic bath. The powder sample was placed into a glass watch, below the LED. The air samples inside the box were collected and analyzed by a photoacoustic transducer system (Briiel and Kjaer Multi-gas Monitor Type 1302) equipped with UA 0982, UA 0984, UA 0987,

SB 0527 filters. The initial amount of MEK injected into the test box was 5 µL. The data collection starts 30sec after the initial injection, in order to account the full vaporization of MEK. The test was conducted in dark and UV-light condition for every sample. The collected data were treated and fitted as apparent second-order kinetics [44], by using Equation (1).
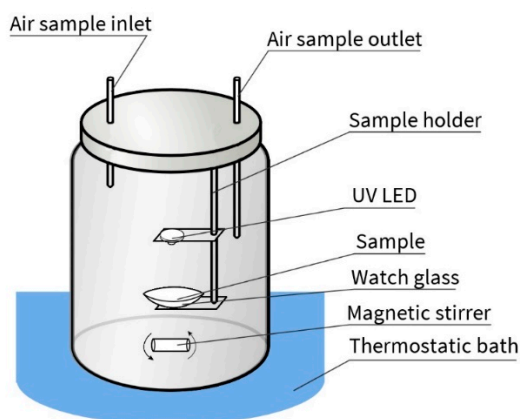

Figure 2. A schematic representation of the reactor used for the methyl ethyl ketone (MEK) removal efficiency in the batch test.

3. Results

3.1. Characterization of the Composite

In Figure 3, the first picture (a) shows the raw silica particles, (b) the silica particle after the TiO_2 hydrothermal deposition (A3), (c) the aggregated particles of TiO_2 P25 and (d) the same over the silica surface (W3, P25 agglomerates are highlighted by the arrows).
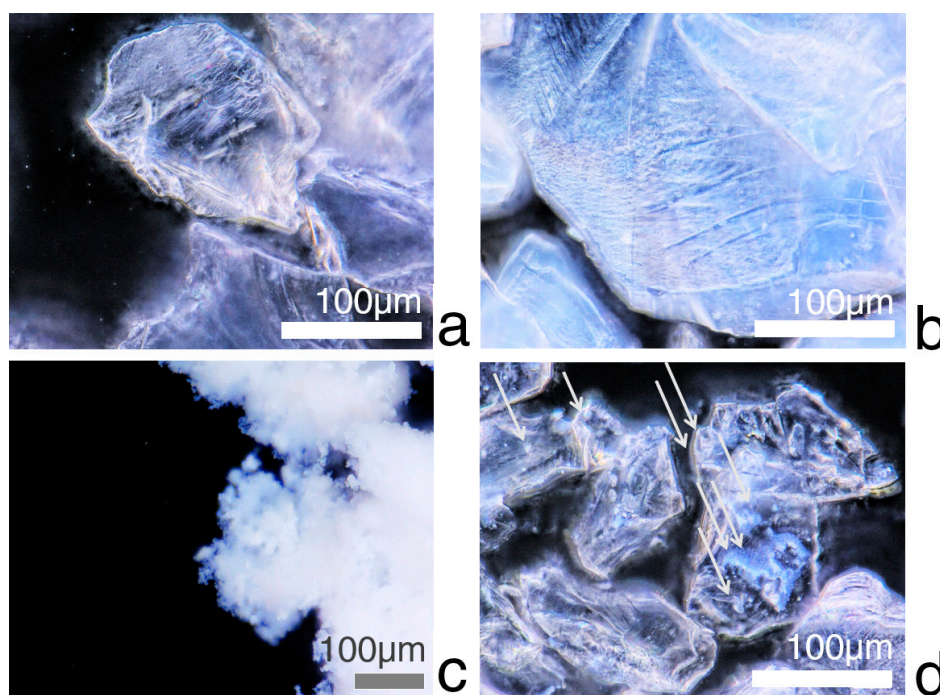

Figure 3. Magnifications of raw silica (**a**), A3 (**b**), P25 (**c**), W3 (**d**).

A magnification of sample A3 obtained by SEM is reported in Figure 4a,b, where TiO_2 particles, within the size of dozen of nanometers, are displaced over the silica surface (See Figure S3, in the

supplementary material, for the primary particle size distributions). The XRD diffractogram for the A3 sample highlights the presence of titanium dioxide in the anatase form.
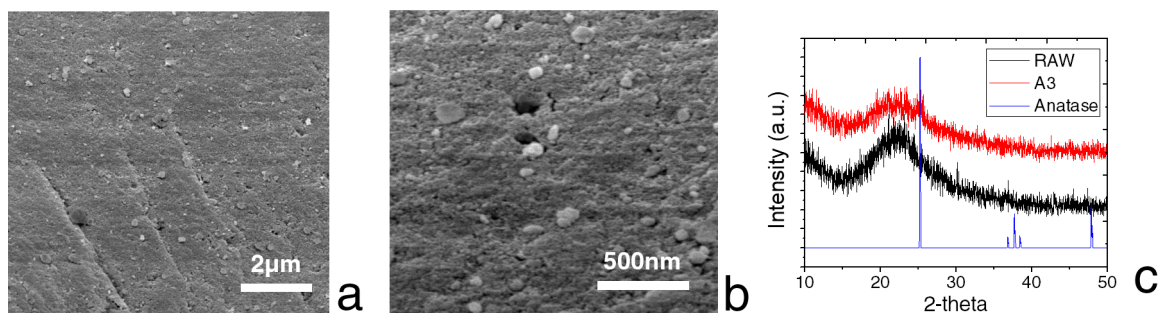

Figure 4. SEM pictures (**a**,**b**) and XRD diffractogram (**c**) of the samples A3.

Nitrogen isotherms and pore size distributions were presented, respectively, in Figures 5 and 6. From Figure 5, for the silica-containing samples, Type IV isotherms with hysteresis loops are obtained, indicating the dominance of mesopores in these samples. The hysteresis loops of pure silica and titania start near relative pressures of 0.45 and 0.85, respectively. However, due to the mutual contribution of pure silica and titania, the hysteresis loops of composites obtained by hydrothermal method (Figure 5a) ranged between the silica and titania ones, while the isotherms of the samples obtained by wet mixing were not strongly affected by the P25 amount.
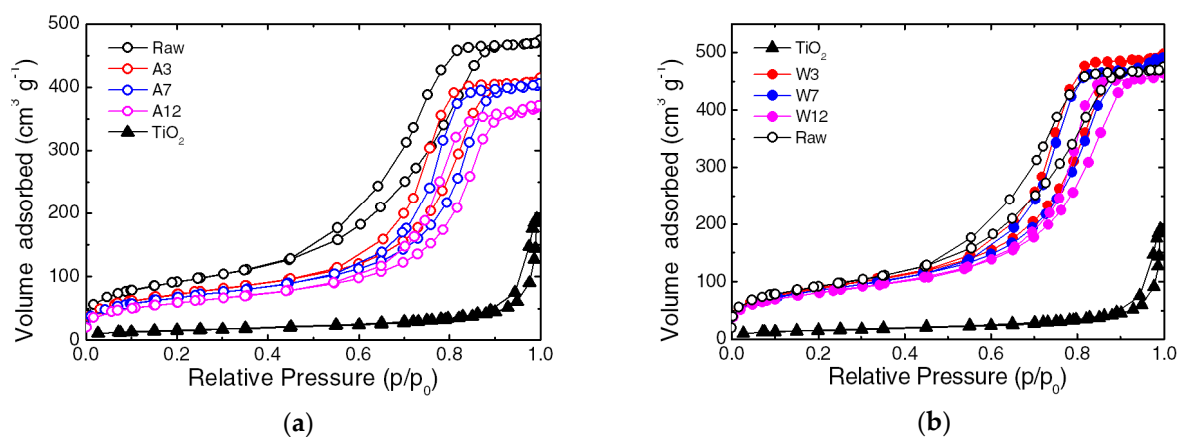

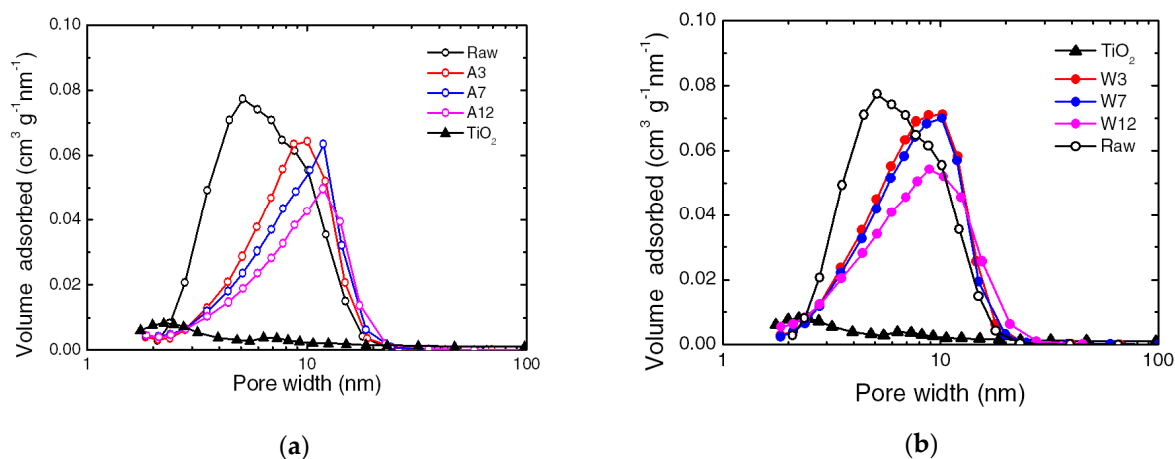**Figure 5.** Nitrogen adsorption isotherms: A-series (**a**) and W-series (**b**).

Figure 6. The pore size distributions: A-series (**a**) and W-series (**b**).

In Figure 6a,b, the pore size distributions of silica-titania composites are similar to pure silica, since titania has a much smaller mass portion. Moreover, a decrease of the volume of nitrogen adsorbed by the smaller porosity is observed, which is slightly more accentuated in the samples obtained by the hydrothermal method.

It can be seen for all the samples the water vapor adsorbed increases sharply during the initial stage (50% of the total capacity in the first 3 min), while it grows slowly as the samples reach saturation. The experimental data reported in Figure 7 has been fitted according to Equation (1) in order to obtain two parameters for easy comparison. Those values are reported in Table 2.
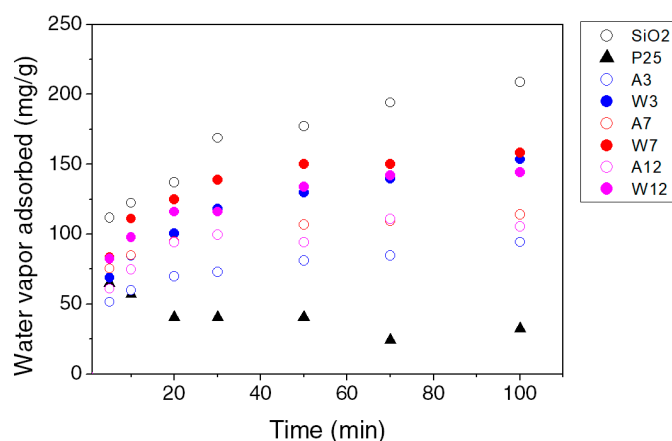

Figure 7. Water vapor adsorption kinetic.

Table 2. The surface area, pore parameters and water vapor adsorption kinetic parameters of prepared samples.

Samples	Texture Properties			Water Vapor Adsorption Kinetic	
	BET Surface Area	Pore Volume	Average Pore Diameter	q_e	h
	$m^2\ g^{-1}$	$cm^3\ g^{-1}$	nm	$mg\ g^{-1}$	$mg\ g^{-1}\ min^{-1}$
SiO_2	327	0.74	9	222	24
TiO_2	54	0.30	22	42	15
A3	258	0.64	10	98	13
A7	241	0.62	10.4	165	15
A12	210	0.57	10.9	117	27
W3	314	0.77	9.8	165	30
W7	302	0.76	10	111	26
W12	288	0.72	10	152	25

The fastest kinetic and capacity of water vapor adsorption belongs to the raw silica sample. The modification of the silica samples mainly lead to a decrease in the maximum capacity, q_e, at the equilibrium of water vapor adsorbed. The samples obtained by the hydrothermal method are the most affected. This aspect is also shown by the decrease of the BET surface area, while h, which is related to the rate constant of sorption, is not strongly influenced by the titania addition.

3.2. Photocatalytic Activity

The samples photocatalytic activity is summarized in Figure 8 and reported in the supplementary material, Table S4. The experimental data were fitted by using equations 1, 2, 3, respectively to determine the MEK, NO and NOx removal rates. The latter two are reported in Figure 8a, where it is possible to distinguish a different trend for the two composites. For the composite obtained by hydrothermal method, a photocatalytic activity maximum is found for the composite having the 3% in

mass of TiO_2, decreasing with increasing TiO_2 load, while for the reference composite, the efficiency increases with increasing the amount of P25 in the sample. Similarly, all the samples having the 3% of TiO_2 belong to the fastest MEK removal kinetic, both under dark (with the only adsorption) and light (with photocatalysis) conditions. By increasing the amount of TiO_2, both adsorption and photocatalysis are negatively affected.
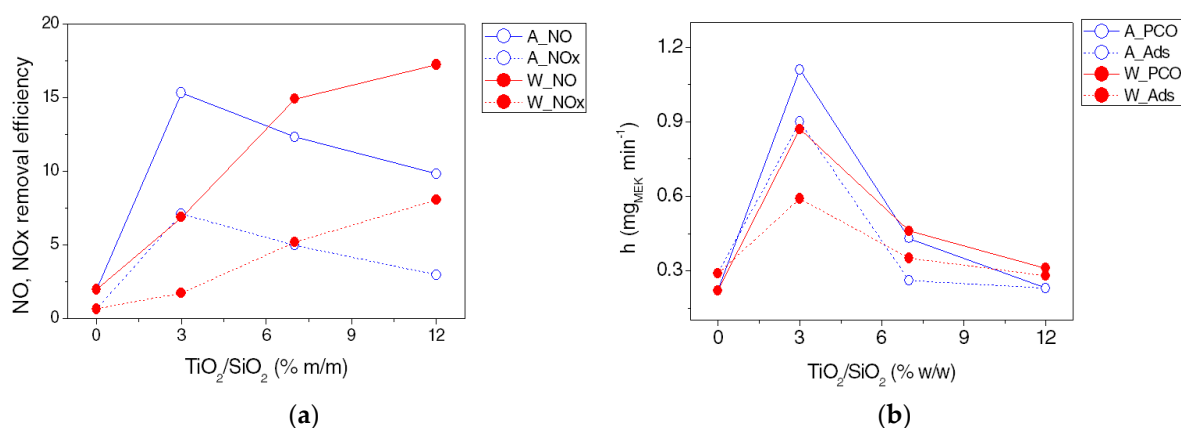

Figure 8. (**a**) NO (solid line) and NOx (dashed line) removal efficiencies for the A (blue) and W (red) composites as a function of the TiO_2 amount. (**b**) MEK removal rate under dark (dashed line) and UV (solid line) conditions for the A (blue) and W (red) composites as a function of the TiO_2 amount.

4. Discussion

After the hydrothermal treatment, the XRD pattern confirms the presence of TiO_2 in anatase crystalline form, associated with a decrease of the BET surface area. The BET surface area's decreasing trend, with the increasing TiO_2 content, is in accordance with the work of other authors [8,16,36,45], and it is due to the partial covering of the porosity by the titania layer formation. Generally, a slight decrease of the TiO_2/SiO_2 surface area implies a good deposition of the TiO_2 particles on the silica gel surface. In this case, for both samples set, a reduction of the volume adsorbed by smaller pores is observed. However, only to the sample obtained by the hydrothermal method corresponds a reduction of the final volume of nitrogen adsorbed. This is because only in the latter one, the titania well covers the silica surface, affecting the composite porosity, while, for the samples obtained by wet mixing, the porosity loss is due to the increasing presence of P25 at the expense of the silica. While balancing the loss of porosity with the acquired photocatalytic properties, it is possible to determine the optimum amount of TiO_2 needed, which, in our study, is close to the 3% *w/w*.

The synthesized SiO_2/TiO_2 composites exhibit a higher water vapor adsorption kinetic than the TiO_2 only, but lower to the silica one. Due to the significant daily and seasonal variation of the indoor humidity levels, porous adsorbent materials can act as a buffer in controlling humidity levels, without adding energy costs to the building due to their hygroscopic abilities. However, an excessive amount of water vapor adsorbed may result in mold growth and biological organisms proliferation. Therefore, TiO_2 can be used both to tune the adsorptive capacity and to provide an antibacterial effect [46].The enhanced adsorption of MEK under dark conditions by the composites can be due both to the formation of new acid sites in the TiO_2–SiO_2 mixed metal oxide [47] and, additionally, to the sulfate modification [48].

5. Conclusions

In this study, a photocatalytic silica/titania composite has been prepared by the hydrothermal method, starting from titanium metal shavings and, through to the development of the acid precursor, titanium dioxide was formed on the silica surface, demonstrating an alternative simple and sustainable route for composite production.

The synthesized composite has excellent hygrometric and adsorptive properties with a photocatalytic activity comparable to the commercial nano-TiO_2. The highest performing composite was the one with the 3% in weight of titania, which implies a dramatic decrease in the amount of raw titanium needed. A fortiori, the use of inexpensive materials, easily available or resulting from secondary manufacturing processes, allows to lower the final cost of the photocatalytic composite, paving the way for its utilization in the building industry. As indoor air quality is a major concern [49], future developments include the investigation of such composites as functional aggregate in plasters and concrete for the indoor air quality enhancement [50] and the partial substitution of silica with fly ashes [51].

Conflicts of Interest: The authors declare no conflicts of interest.

References

1.　R.S.C. TiO2: Manufacture of Titanium Dioxide. *RSC Adv. Chem. Sci.* **2016**, *5*, 2.

2.　Gázquez, M.J.; Bolívar, J.P.; Garcia-Tenorio, R.; Vaca, F. A Review of the Production Cycle of Titanium Dioxide Pigment. *Mater. Sci. Appl.* **2014**, *5*, 441–458. [CrossRef]

3.　Hakki, A.; Yang, L.; Wang, F.; Macphee, D.E. The Effect of Interfacial Chemical Bonding in TiO2-SiO2 Composites on Their Photocatalytic NOx Abatement Performance. *J. Vis. Exp.* **2017**. [CrossRef] [PubMed]

4.　Zhang, Q.; Bao, N.; Wang, X.; Hu, X.; Miao, X.; Chaker, M.; Ma, D. Advanced Fabrication of Chemically Bonded Graphene/TiO2 Continuous Fibers with Enhanced Broadband Photocatalytic Properties and Involved Mechanisms Exploration. *Sci. Rep.* **2016**, *6*, 38066. [CrossRef] [PubMed]

5.　Sellappan, R. *Mechanisms of Enhanced Activity of Model TiO2/Carbon and TiO2/Metal Nanocomposite Photocatalysts*; Department of Applied Physics Chalmers, University of Technology: Göteborg, Sweden, 2013; ISBN 9789173858717.

6.　Pierpaoli, M.; Lewkowicz, A.; Ficek, M.; Ruello, M.L.; Bogdanowicz, R. Preparation and characterization of TiO2/carbon nanowall composite on a transparent substrate. *Photonics Lett. Pol.* **2018**, *10*, 54–56. [CrossRef]

7.　Stöber, W.; Fink, A.; Bohn, E. Controlled growth of monodisperse silica spheres in the micron size range. *J. Colloid Interface Sci.* **1968**, *26*, 62–69. [CrossRef]

8.　Anderson, C.; Bard, A.J. Improved Photocatalytic Activity and Characterization of Mixed TiO2/SiO2 and TiO2/Al2O3 Materials. *J. Phys. Chem. B* **1997**, *101*, 2611–2616. [CrossRef]

9.　Dutoit, D.C.M.; Schneider, M.; Baiker, A. Titania-Silica Mixed Oxides: I. Influence of Sol-Gel and Drying Conditions on Structural Properties. *J. Catal.* **1995**, *153*, 165–176. [CrossRef]

10.　Xianzhi, F.U.; Clark, L.A.; Yang, Q.; Anderson, M.A.; Fu, X.; Clark, L.A.; Yang, Q.; Anderson, M.A. Enhanced photocatalytic performance of titania-based binary metal oxides: TiO2/SiO2 and TiO2/ZrO2. *Environ. Sci. Technol.* **1996**, *30*, 647–653. [CrossRef]

11.　Aguado, J.; Vangrieken, R.; López-Muñoz, M.; Marugan, J.; López-Muñoz, M.-J.; Marugan, J.; van Grieken, R.; López-Muñoz, M.-J.; Marugán, J. A comprehensive study of the synthesis, characterization and activity of TiO2 and mixed TiO2/SiO2 photocatalysts. *Appl. Catal. A Gen.* **2006**, *312*, 202–212. [CrossRef]

12.　Kochkar, H.; Figueras, F. Synthesis of Hydrophobic TiO2–SiO2Mixed Oxides for the Epoxidation of Cyclohexene. *J. Catal.* **1997**, *171*, 420–430. [CrossRef]

13.　Li, X.; He, J. Synthesis of Raspberry-Like SiO–TiO2 Nanoparticles toward Antireflective and Self-Cleaning Coatings. *ACS Appl. Mater. Interfaces* **2013**, *5*, 5282–5290. [CrossRef] [PubMed]

14.　Guo, N.; Liang, Y.; Lan, S.; Liu, L.; Ji, G.; Gan, S.; Zou, H.; Xu, X. Uniform TiO2–SiO2 hollow nanospheres: Synthesis, characterization and enhanced adsorption–photodegradation of azo dyes and phenol. *Appl. Surf. Sci.* **2014**, *305*, 562–574. [CrossRef]

15.　Dong, W.; Sun, Y.; Lee, C.W.; Hua, W.; Lu, X.; Shi, Y.; Zhang, S.; Chen, J.; Zhao, D. Controllable and Repeatable Synthesis of Thermally Stable Anatase Nanocrystal−Silica Composites with Highly Ordered Hexagonal Mesostructures. *J. Am. Chem. Soc.* **2007**, *129*, 13894–13904. [CrossRef] [PubMed]

16.　Li, Y.; Kim, S.J. Synthesis and Characterization of Nano titania Particles Embedded in Mesoporous Silica with Both High Photocatalytic Activity and Adsorption Capability. *J. Phys. Chem. B* **2005**, *109*, 12309–12315. [CrossRef] [PubMed]

17.　Beyers, E.; Biermans, E.; Ribbens, S.; De Witte, K.; Mertens, M.; Meynen, V.; Bals, S.; Van Tendeloo, G.; Vansant, E.F.; Cool, P. Combined TiO2/SiO2 mesoporous photocatalysts with location and phase controllable TiO2 nanoparticles. *Appl. Catal. B Environ.* **2009**, *88*, 515–524. [CrossRef]

18.　van Grieken, R.; Aguado, J.; López-Muñoz, M.J.; Marugán, J. Synthesis of size-controlled silica-supported TiO2 photocatalysts. *J. Photochem. Photobiol. A Chem.* **2002**, *148*, 315–322. [CrossRef]

19.　Itoh, M.; Hattori, H.; Tanabe, K. The acidic properties of TiO2-SiO2 and its catalytic activities for the amination of phenol, the hydration of ethylene and the isomerization of butene. *J. Catal.* **1974**, *35*, 225–231. [CrossRef]

20.　Nilchi, A.; Janitabar-Darzi, S.; Mahjoub, A.R.; Rasouli-Garmarodi, S. New TiO2/SiO2 nanocomposites—Phase transformations and photocatalytic studies. *Colloids Surf. Physicochem. Eng. Asp.* **2010**, *361*, 25–30. [CrossRef]

21.　Yang, Z.; Xu, Y.; Yang, S. Fabrication, characterization, and photocatalytic performance of TiO2 hybridized with SiO2. *Russ. J. Appl. Chem.* **2016**, *89*, 2050–2060. [CrossRef]

22.　Zhang, X.; Zhang, F.; Chan, K.-Y. Synthesis of titania–silica mixed oxide mesoporous materials, characterization and photocatalytic properties. *Appl. Catal. A Gen.* **2005**, *284*, 193–198. [CrossRef]

23.　Xie, C.; Xu, Z.; Yang, Q.; Xue, B.; Du, Y.; Zhang, J. Enhanced photocatalytic activity of titania–silica mixed oxide prepared via basic hydrolyzation. *Mater. Sci. Eng. B* **2004**, *112*, 34–41. [CrossRef]

24.　Bellardita, M.; Addamo, M.; Di Paola, A.; Marcì, G.; Palmisano, L.; Cassar, L.; Borsa, M. Photocatalytic activity of TiO2/SiO2 systems. *J. Hazard. Mater.* **2010**, *174*, 707–713. [CrossRef] [PubMed]

25.　Belhekar, A.A.; Awate, S.V.; Anand, R. Photocatalytic activity of titania modified mesoporous silica for pollution control. *Catal. Commun.* **2002**, *3*, 453–458. [CrossRef]

26.　Leboda, R.; Gun'ko, V.; Marciniak, M.; Malygin, A.; Malkin, A.; Grzegorczyk, W.; Trznadel, B.; Pakhlov, E.; Voronin, E. Structure of Chemical Vapor Deposition Titania/Silica Gel. *J. Colloid Interface Sci.* **1999**, *218*, 23–39. [CrossRef]

27.　Li, Z.; Hou, B.; Xu, Y.; Wu, D.; Sun, Y. Hydrothermal synthesis, characterization, and photocatalytic performance of silica-modified titanium dioxide nanoparticles. *J. Colloid Interface Sci.* **2005**, *288*, 149–154. [CrossRef]

28.　Anpo, M.; Nakaya, H.; Kodama, S.; Kubokawa, Y.; Domen, K.; Onishi, T. Photocatalysis over binary metal oxides. Enhancement of the photocatalytic activity of titanium dioxide in titanium-silicon oxides. *J. Phys. Chem.* **1986**, *90*, 1633–1636. [CrossRef]

29.　He, C.; Tian, B.; Zhang, J. Thermally stable SiO2-doped mesoporous anatase TiO2 with large surface area and excellent photocatalytic activity. *J. Colloid Interface Sci.* **2010**, *344*, 382–389. [CrossRef]

30.　Inumaru, K.; Kasahara, T.; Yasui, M.; Yamanaka, S. Direct nanocomposite of crystalline TiO2 particles and mesoporous silica as a molecular selective and highly active photocatalyst. *Chem. Commun.* **2005**, *16*, 2131–2133. [CrossRef]

31.　Paušová, Š.; Krýsa, J.; Jirkovský, J.; Prevot, V.; Mailhot, G. Preparation of TiO2-SiO2 composite photocatalysts for environmental applications. *J. Chem. Technol. Biotechnol.* **2014**, *89*, 1129–1135. [CrossRef]

32.　Smitha, V.S.; Manjumol, K.A.; Baiju, K.V.; Ghosh, S.; Perumal, P.; Warrier, K.G.K. Sol–gel route to synthesize titania-silica nano precursors for photoactive particulates and coatings. *J. Sol-Gel Sci. Technol.* **2010**, *54*, 203–211. [CrossRef]

33.　Alaoui, O.T.; Nguyen, Q.T.; Rhlalou, T. Preparation and characterization of a new TiO2/SiO2 composite catalyst for photocatalytic degradation of indigo carmin. *Environ. Chem. Lett.* **2009**, *7*, 175–181. [CrossRef]

34.　Hirano, M.; Ota, K.; Inagaki, M.; Iwata, H. Hydrothermal Synthesis of TiO2/SiO2 Composite Nanoparticles and Their Photocatalytic Performances. *J. Ceram. Soc. Jpn.* **2004**, *112*, 143–148. [CrossRef]

35.　Montes, M.; Getton, F.P.; Vong, M.S.W.; Sermon, P.A. Titania on silica. A comparison of sol-gel routes and traditional methods. *J. Sol-Gel Sci. Technol.* **1997**, *8*, 131–137. [CrossRef]

36. Hirano, M.; Ota, K.; Iwata, H. Direct Formation of Anatase (TiO2)/Silica (SiO2) Composite Nanoparticles with High Phase Stability of 1300 °C from Acidic Solution by Hydrolysis under Hydrothermal Condition. *Chem. Mater.* **2004**, *16*, 3725–3732. [CrossRef]

37. Hirano, M.; Ota, K. Preparation of photoactive anatase-type TiO2/silica gel by direct loading anatase-type TiO2 nanoparticles in acidic aqueous solutions by thermal hydrolysis. *J. Mater. Sci.* **2004**, *39*, 1841–1844. [CrossRef]

38. Grubb, G.F.; Bakshi, B.R. Life Cycle of Titanium Dioxide Nanoparticle Production. *J. Ind. Ecol.* **2011**, *15*, 81–95. [CrossRef]

39. Middlemas, S.; Fang, Z.Z.; Fan, P. Life cycle assessment comparison of emerging and traditional Titanium dioxide manufacturing processes. *J. Clean. Prod.* **2015**, *89*, 137–147. [CrossRef]

40. Babaizadeh, H.; Hassan, M. Life cycle assessment of nano-sized titanium dioxide coating on residential windows. *Constr. Build. Mater.* **2013**, *40*, 314–321. [CrossRef]

41. Giosuè, C.; Pierpaoli, M.; Mobili, A.; Ruello, M.L.; Tittarelli, F. Influence of binders and lightweight aggregates on the properties of cementitious mortars: From traditional requirements to indoor air quality improvement. *Materials (Basel)* **2017**, *10*, 978. [CrossRef]

42. Bondarenko, V.; Ruello, M.L.; Bondarenko, A. Ageing of Photocatalytic Materials: Investigation, Assessment and Possible Solving. *Chem. Eng. Trans.* **2016**, *47*, 133–138. [CrossRef]

43. Pierpaoli, M.; Giosuè, C.; Ruello, M.L.; Fava, G. Appraisal of a hybrid air cleaning process. *Environ. Sci. Pollut. Res.* **2017**, *24*, 12638–12645. [CrossRef] [PubMed]

44. Pierpaoli, M.; Ruello, M.; Fava, G. Enhanced Adsorption of Organic Compounds over an Activated Carbon Cloth by an External-Applied Electric Field. *Environments* **2017**, *4*, 33. [CrossRef]

45. Machida, M.; Norimoto, K.; Watanabe, T.; Hashimoto, K.; Fujishima, A. Effect of SiO2 addition in super-hydrophilic property of TiO2 photocatalyst. *J. Mater. Sci.* **1999**, *34*, 2569–2574. [CrossRef]

46. Dunford, R.; Salinaro, A.; Cai, L.; Serpone, N.; Horikoshi, S.; Hidaka, H.; Knowland, J. Chemical oxidation and DNA damage catalysed by inorganic sunscreen ingredients. *FEBS Lett.* **1997**, *418*, 87–90. [CrossRef]

47. Jung, S.M.; Dupont, O.; Grange, P. TiO2–SiO2 mixed oxide modified with H2SO4: I. Characterization of the microstructure of metal oxide and sulfate. *Appl. Catal. A Gen.* **2001**, *208*, 393–401. [CrossRef]

48. Tanabe, K.; Misono, M.; Hattori, H.; Ono, Y. *New Solid Acids and Bases: Their Catalytic Properties*; Kodansha: Bunkyō, Tokyo, Japan, 1989; Volume 51, ISBN 9780080887555.

49. Pierpaoli, M.; Ruello, M.L. Indoor Air Quality: A Bibliometric Study. *Sustainability* **2018**, *2018 10*, 3830. [CrossRef]

50. Tittarelli, F.; Giosuè, C.; Mobili, A.; Ruello, M.L. Influence of binders and aggregates on VOCs adsorption and moisture buffering activity of mortars for indoor applications. *Cem. Concr. Compos.* **2015**, *57*, 75–83. [CrossRef]

51. Fava, G.; Naik, T.; Pierpaoli, M.; Fava, G.; Naik, T.R.; Pierpaoli, M. Compressive Strength and Leaching Behavior of Mortars with Biomass Ash. *Recycling* **2018**, *3*, 46. [CrossRef]